Marine and Petroleum Geology 104 (2019) 190–199

Contents lists available at ScienceDirect

Marine and Petroleum Geology

journal homepage: www.elsevier.com/locate/marpetgeo

Research paper

CO_2 sequestration by mineral trapping in natural analogues in the Yinggehai Basin, South China Sea

Rui Liu[a,b,*], Niklas Heinemann[c], Jianzhang Liu[b], Weilin Zhu[d], Mark Wilkinson[c], Yuhong Xie[e], Zhenfeng Wang[e], Tao Wen[f], Fang Hao[b], R. Stuart Haszeldine[c]

[a] School of Geoscience and Technology, Southwest Petroleum University, Chengdu, 610500, China
[b] Key Laboratory of Tectonics and Petroleum Resources (China University of Geosciences), Ministry of Education, Wuhan, 430074, China
[c] University of Edinburgh, School of Geosciences, Grant Institute, West Main Road, Edinburgh, EH9 3JW, UK
[d] China National Offshore Oil Corporation (CNOOC), Beijing, 100010, China
[e] Zhanjiang Branch of CNOOC Ltd, Zhanjiang, 524057, China
[f] Earth and Environmental Systems Institute, Pennsylvania State University, University Park, 16802, USA

ARTICLE INFO

Keywords:
CO_2 geological storage
Mineral trapping
Reservoir overpressure
Yinggehai basin

ABSTRACT

Mineral trapping of CO_2 by precipitation of carbonate minerals is seen as the most permanent and secure mechanism of CO_2 storage. We have investigated mineral trapping in CO_2-rich siliciclastic reservoirs of the Upper Miocene age in the Yinggehai Basin (South China Sea) and used nearby CO_2-poor reservoirs of similar age as benchmarks for the analysis. Within the reservoir, the CO_2 has triggered the reaction from calcite plus chlorite to ankerite plus kaolinite, which traps 5 mol of CO_2 per mole of chlorite. Geochemical modelling shows that the total amount of permanently trapped CO_2 is approximately one half of the CO_2 in the newly formed ankerite. Caprock mineralogy shows that CO_2 leakage has occurred and CO_2 has migrated into the shale-rich caprock, but without loss of caprock integrity.

1. Introduction

China was reported to contribute about one-third of fossil-fuel CO_2 emission among all countries by 2014 (Boden et al., 2017; The Netherlands Environmental Assessment Agency, 2007). The injection and storage of CO_2 into subsurface reservoirs is considered a vital technology to reduce CO_2 emissions from coal-fired power plants and other industrial sources (IPCC, 2005; Bickle, 2009). The presence of saline aquifers as large-scale CO_2 sinks close to industrial areas is key to enabling carbon capture and storage (CCS) delivery in China. The Yinggehai Basin is located in the South China Sea close to the Guangdong province with a population of more than 110 million and a massive industrial sector. To date, the Pearl River Mouth Basin, to the northeast of the Yinggehai Basin, has been investigated for CO_2 storage (Zhou et al., 2011; Heinemann et al., 2017, 2018) but so far there has been no investigation into the long-term fate of injected CO_2, especially on mineral trapping, in the entire South China Sea.

When massive volumes of CO_2 are injected into a reservoir for storage purposes, the chemical equilibrium of the system will change and both precipitation and dissolution of minerals can be triggered. The investigation of natural analogues for CO_2 storage where CO_2 has naturally accumulated in the subsurface, helps to predict what reactions will take place when anthropogenic CO_2 is injected into the subsurface, and if these reactions are for the benefit or a disadvantage for long-term CO_2 storage. A major problem when studying natural analogues is to distinguish between minerals precipitated during burial diagenesis before the CO_2 enters the reservoir, and minerals that precipitated directly due to the high CO_2 concentration (Heinemann et al., 2013). Previous investigations on natural analogues, such as the Fizzy Field in the southern North Sea, UK (Wilkinson et al., 2009), compared the results with a nearby non-CO_2 containing reservoir of similar stratigraphic age (Heinemann et al., 2013). By using a reference reservoir without CO_2, the confidence of the interpretation increases significantly and allows mineral trapping to be quantified.

In this study, we undertake the first investigation of mineral trapping in Miocene siliciclastic reservoirs of the Yinggehai Basin on the northwestern South China Sea (Fig. 1). We compare two natural reservoirs, one filled with a CO_2-rich gas phase and one with hydrocarbon gas located relatively close to each other and of similar stratigraphic age. We analyze the pressure system, the mineralogy, and the stable-

* Corresponding author. School of Geoscience and Technology, Southwest Petroleum University, No. 8, Xindu Road, Xindu District, Chengdu, 610500, Sichuan Province, China.
E-mail address: liurui@outlook.com (R. Liu).

https://doi.org/10.1016/j.marpetgeo.2019.03.018
Received 19 August 2018; Received in revised form 13 March 2019; Accepted 13 March 2019
Available online 16 March 2019
0264-8172/

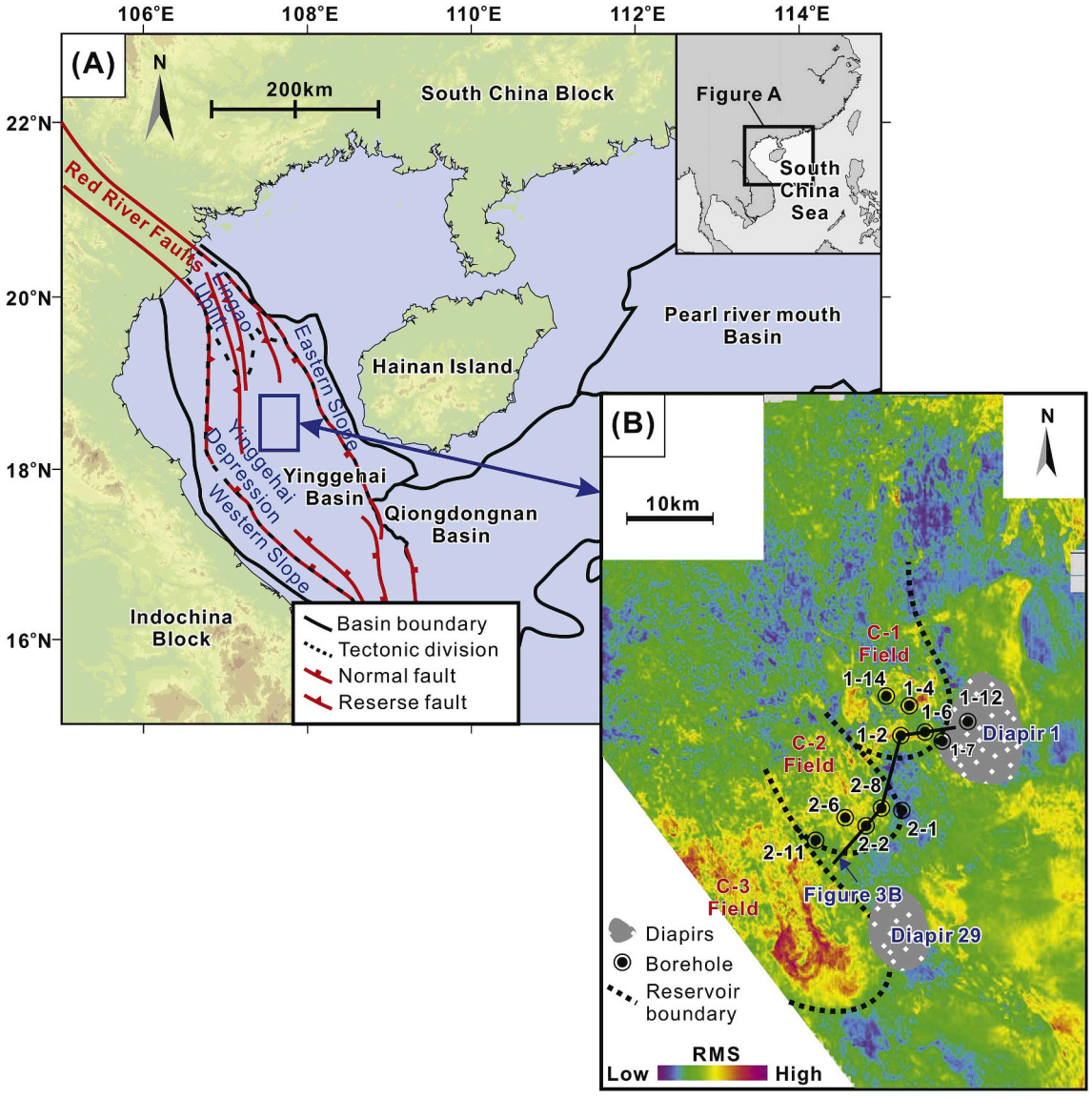

Fig. 1. (A) Tectonic setting of the Yinggehai Basin and surrounding region. (B) The root mean square amplitude extracted from the Upper Miocene of the study area, showing the distribution of siliciclastic reservoirs. The black circles denote the locations of wells.

isotope ratios of the carbonate minerals to reveal if, and for how long, the precipitation of carbonate minerals as triggered by an increase in CO_2 concentration, has taken place. The results will not only give valuable insights into potential mineral reactions in the presence of CO_2 but will also help to evaluate if the Yinggehai Basin in China is a safe storage site for anthropogenic CO_2.

2. Geological setting

2.1. The Yinggehai Basin

The Yinggehai Basin lies on the continental shelf between the Hainan Island of China and the eastern coast of Vietnam, and mainly comprises of the Yinggehai Depression, Eastern and Western Slopes, and Lingao Uplift (Fig. 1A). The Yinggehai Basin formed during the Early Cenozoic as a response to the motion of South China and Indochina blocks as well as the opening of the South China Sea (Morley, 2002, 2013; Zhu et al., 2009; Lei et al., 2011; Liu et al., 2016). As one of the deepest basins in SE Asia, the Yinggehai Basin comprises clastic sedimentary basin-fill up to 17 km thick, separated into the Paleogene syn-rift and the Neogene post-rift sequences by a regional unconformity (Fig. 2) (Gong and Li, 1997). During the Early Miocene and the Pliocene–Quaternary the sedimentation rate was very high with up to 700 m/Ma (Hao et al., 2000; Lei et al., 2011). Extensive vertical venting structures, such as pipes and gas chimneys, imply the frequent expulsion of overpressure fluids (Lei et al., 2011; Liu et al., 2015), presumably linked to the high sedimentation rates in the Miocene (Luo et al., 2003). Gas pools with CO_2 content varying from < 1 mol% to 93 mol% are widely distributed in the Yinggehai Basin (Hao et al., 2000; Huang et al., 2002, 2004, 2015).

2.2. The Upper Miocene siliciclastic reservoirs

The Upper Miocene siliciclastic reservoirs have yielded some of the most significant gas discoveries in the Yinggehai Basin in the last decade, including the C-1 and C-2 gas fields on the northern Yinggehai Depression (Figs. 1B and 3) (Xie and Huang, 2014; Tong et al., 2015). The C-1 and the C-2 fields comprise of several individual reservoir sands (Fig. 4). The reservoirs of the two fields will be named “C-1 reservoirs” and “C-2 reservoirs” throughout this publication. The CO_2 content in the C-1 reservoirs is up to 70 mol%, but no more than 3 mol% in the C-2 reservoirs (Huang et al., 2015; Liu, 2016) (Fig. 4). Current

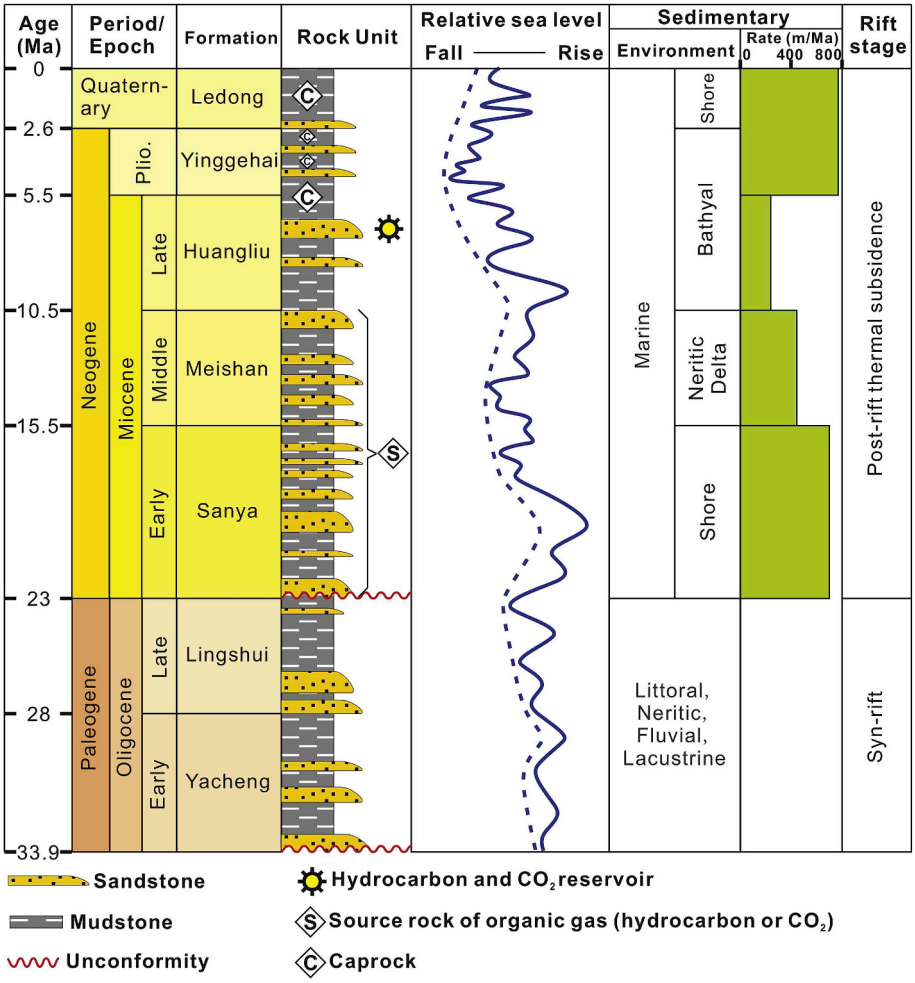

Fig. 2. Generalized stratigraphic section of the Yinggehai Basin. The sedimentation rate data were compiled from Lei et al. (2011), the source-reservoir-caprock system of this study was compiled from Hao et al. (2000) and Huang et al. (2004, 2015).

burial depth (below sea level) of the Upper Miocene reservoirs roughly ranges from 2600 m to 3100 m in the C-1 field, and from 2900 m to 3400 m in the C-2 field (Fig. 4). Hydraulic fractures and episodic fluid expulsions have disturbed the seismic reflectors on the crest of the C-1 field (Liu et al., 2015) (Fig. 3). The reservoir temperatures of the two fields fall on a temperature gradient of 39 °C/km with a surface temperature of approximately 18 °C, as established by Hao et al. (2000) (Fig. 5). The pressure and temperature conditions of both fields exceed the critical point of CO_2 (7.38 MPa, 31.1 °C), and hence CO_2 is present as a supercritical phase.

The Upper Miocene reservoir sandstones of both fields were sourced from the west, delivered by gravity flow, and deposited on the basin floor as channel-lobe complexes during a sea level fall in the late Miocene (Fig. 2) (Zhang et al., 2013; Sun et al., 2014; Cao et al., 2015; Jiang et al., 2015a). These sandstones are predominantly gray or white and contain more than 55 vol% of detrital quartz grains (Zhang et al.,

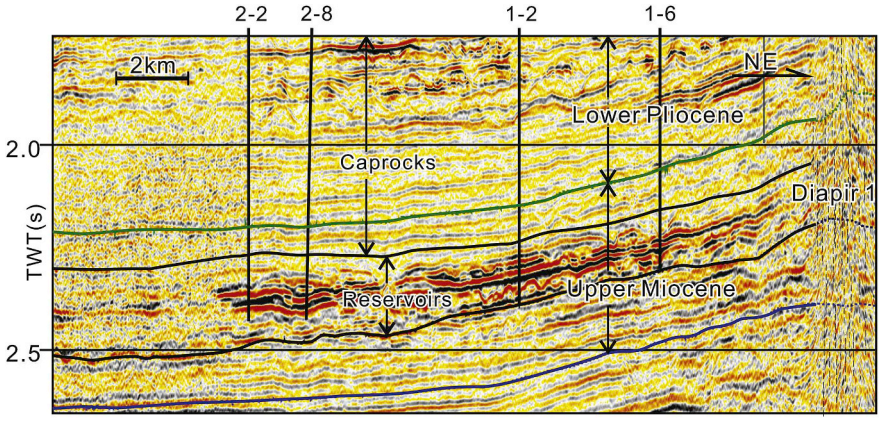

Fig. 3. Seismic sections show the stratigraphic correlation of the Upper Miocene reservoirs (channel-lobe sandstones) and caprocks. Please see Fig. 1B for section locations. TWT is two-way travel time.

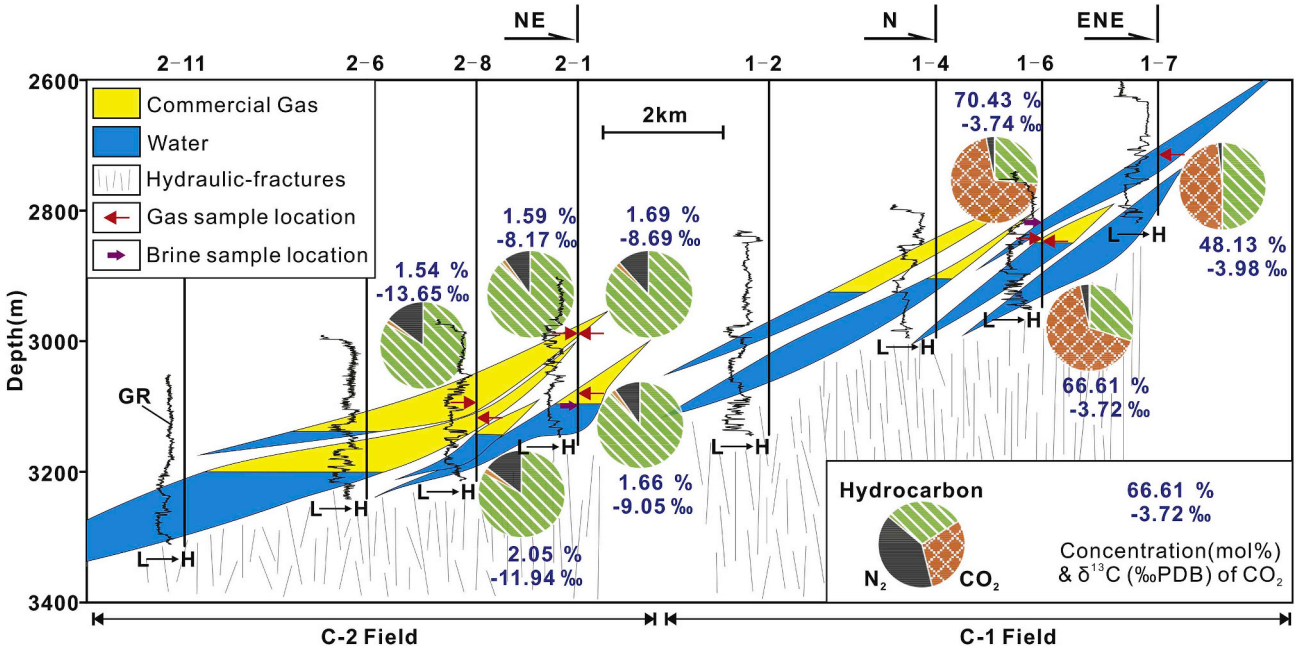

Fig. 4. Well cross-section of the C-1 and C-2 fields including GR (gamma ray) logs. Please see Fig. 1B for well locations. The commercial gas distributions were adapted from Xie and Huang (2014) and Tong et al. (2015). Note that gas phase occurs in well 1–7 but is not enough for commercial production. The concentration and carbon isotopes of CO_2 were derived from Liu (2016). The drawn hydraulic fractures underlying the two fields were the conduits of hydrocarbon/CO_2-charging (Tong et al., 2015).

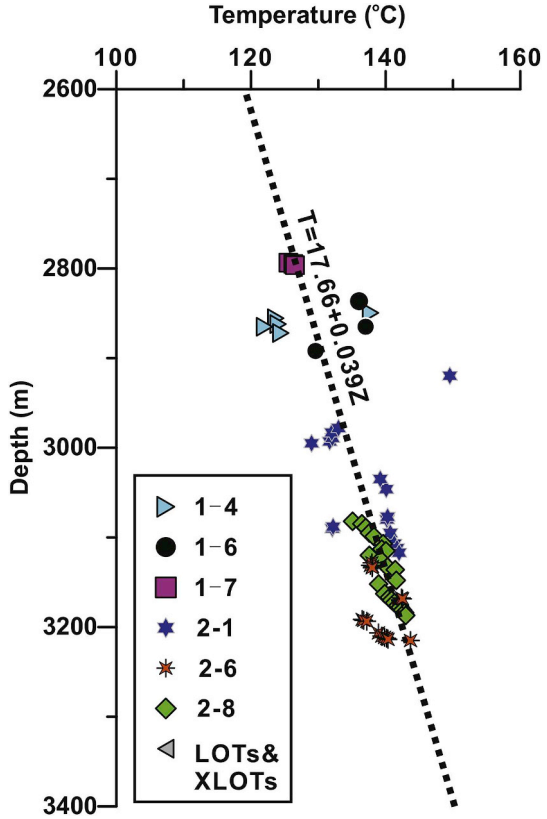

Fig. 5. Temperature versus depth in the C-1 and C-2 field. The temperature gradient is taken from Hao et al. (2000) and plotted as a black line.

2013). K-feldspar dissolution is widely identified in the reservoirs of both fields and carbonate minerals are the predominant cements (Zhang et al., 2013). The Upper Miocene reservoir formations were tilted and uplifted due to the rise of diapirs which began at the end of the Miocene (Figs. 3 and 4) (Liu et al., 2015). Pliocene marine mudstones sourced from the Red River Provenance are the regional caprock overlying the Upper Miocene reservoirs of the two fields (Jiang et al., 2015a) (Figs. 3 and 4).

3. Methodology

A total of 20 sandstone cores (for locations see Figs. 1 and 4) from the gas zone of the Upper Miocene reservoirs were quantitatively analyzed for whole-rock and clay fraction mineralogy, using random-powder X-ray diffraction (XRD). Caprock samples were obtained from two wells (1–12 and 2–1, Fig. 1) located on the crests of the two fields. Mudstone drill cuttings of regional caprock (Pliocene marine mudstone) were analyzed for the clay fraction mineralogy. Procedures for sample preparation, analysis and interpretation were adapted from Moore and Reynolds (1997) and Hillier (2003).

The subset sandstone cores selected from the gas zone were also powdered and acidulated (overnight reaction with 100% phosphoric acid at 70 °C) to extract CO_2. The extracted CO_2 was dried, purified, and analyzed on a MAT253 (Thermo Scientific®) isotope ratio mass spectrometer. Isotopic values are reported relative to Peedee belemnite (PDB), expressed in per mil.

Four brine samples in the Upper Miocene reservoirs (3 from the C-1 reservoirs and 1 from in the C-2 reservoirs) were collected during drill stem tests (DST) and modular dynamic tests (MDT). Chemical composition was determined using industry standard techniques (SY 5523–2000 of CNOOC) (Jiang et al., 2015b).

Mineral reactions within the sandstone were modeled using PHREEQC v. 3.4.0 (http://wwwbrr.cr.usgs.gov/projects/GWC_coupled/phreeqc/index.html) at 130 °C and 50 MPa total pressure. The partial pressure of CO_2 was altered to simulate 1–50 mol% CO_2 in the free-gas phase (fixed partial pressure), with calcite and chlorite (14 Å) as reactants, and dolomite and kaolinite as possible products. Ankerite is not present in the PHREEQC thermodynamic database, hence the use of dolomite. The chlorite (14 Å) phase also has only Mg as a cation (though authigenic chlorite in sediments is commonly Fe-bearing). The modelling is hence of a Fe-free system, which is presented

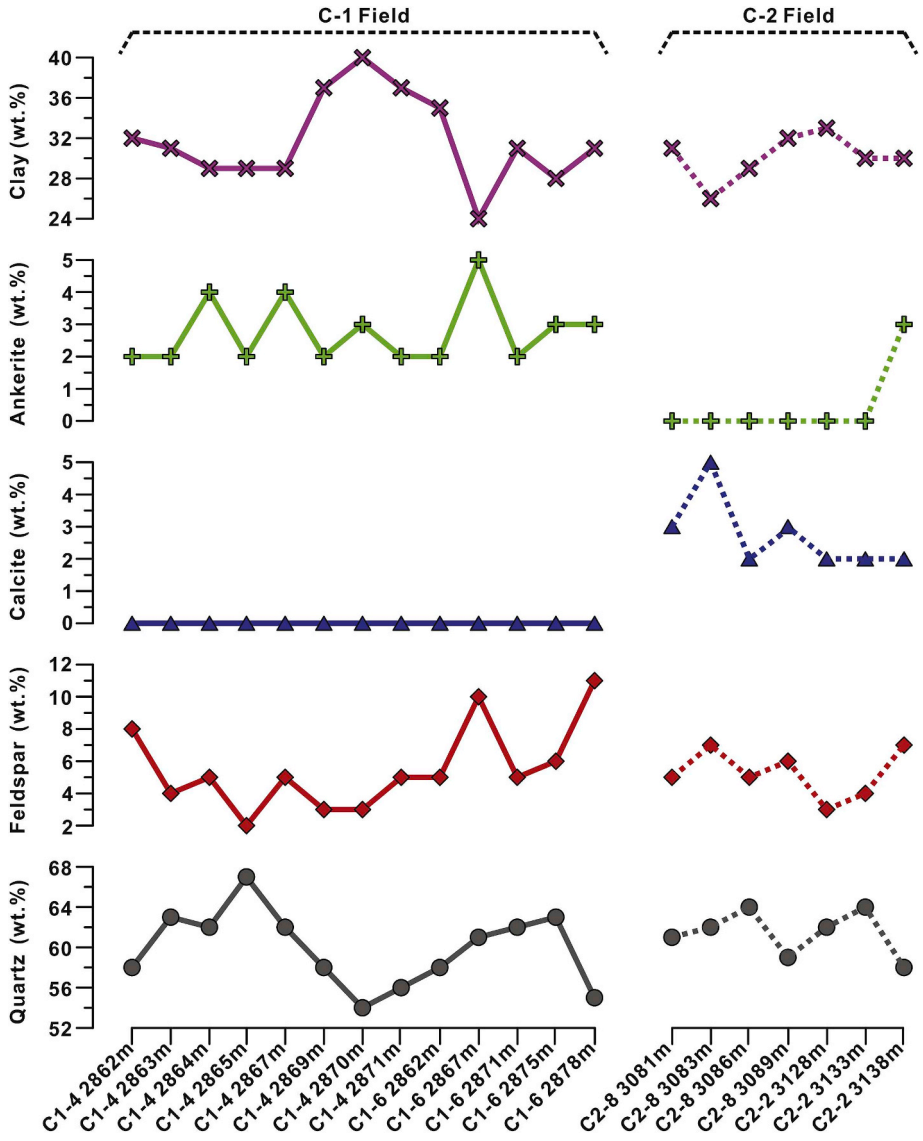

Fig. 6. Results of the whole rock XRD analysis of the Upper Miocene sandstone reservoirs in the C-1 and C-2 fields. Note the distinct difference of the carbonate mineralogy in the C-2 and C-1 reservoirs with calcite dominating in the C-1 and ankerite dominating in the C-2.

as an approximation to the real system where Fe and Mg are the dominant cations.

4. Results

4.1. Reservoir and caprock mineralogy

The Upper Miocene sandstone reservoirs of the C-1 and C-2 fields comprise predominantly quartz, with subordinate clay, feldspars, and carbonates (Fig. 6). Mean quartz values of 60 ± 4 wt% and 61 ± 2 wt % occur in the C-1 and C-2 reservoirs, respectively. Calcite and ankerite vary significantly between the reservoirs of the two fields (Fig. 6 and Table 1). C-1 reservoirs are rich in ankerite (3 ± 1 wt%), but lack of calcite. In contrast, C-2 reservoirs are generally rare in ankerite and rich in calcite (3 ± 2 wt%).

Fig. 7 shows the results of the XRD analysis of the clay minerals in both reservoirs. Chlorite is the dominant clay mineral (57 ± 3 wt%) in the C-2 reservoirs, but only a negligible amount of chlorite is developed in the C-1 reservoirs. Kaolinite has a dominance of 61 ± 6 wt% in the C-1 reservoirs, but it is absent in the C-2 reservoirs. The sum of illite and illite/smectite mixed layers is 37 ± 7 wt% and 43 ± 3 wt% in the C-1 and C-2 reservoirs, respectively.

Clay minerals of the Pliocene mudstone caprock consist of chlorite, kaolinite, illite, and illite/smectite mixed layers in wells 1–12 (C-1) and 2–1 (C-2) (Fig. 8). The results from the analyses show that the proportion of chlorite is lower and the proportion of kaolinite is higher in well 1–12 compared to well 2–1. The proportion of illite increases with burial depth whereas the proportion of illite/smectite mixed layers decreases. However, the total sum of illite and illite/smectite mixed layers shows no distinct difference between the two wells.

4.2. Carbon and oxygen stable-isotopic ratios of reservoir

The $\delta^{13}C$ and $\delta^{18}O$ values of carbonate minerals in the reservoirs of the two fields are shown in Fig. 9. $\delta^{13}C$ and $\delta^{18}O$ in the C-1 reservoirs are approximately constant at −10.05 ‰PDB and −2.07 ‰PDB, respectively. Whereas $\delta^{13}C$ (ranges from −4.19 to −2.76 ‰PDB) positively correlated with $\delta^{18}O$ (ranges from −9.93 to −6.71 ‰PDB) in the C-2 reservoirs.

Table 1
Systematical comparison between the C-1 and the C-2 field.

Parameter			C-1 Field	C-2 Field
Reservoir	Dominant Gas		CO_2	Hydrocarbons
	Water table height		≥2/3rds of reservoir height	≤1/2nds of reservoir height
	CO_2	Concentration	48.13–70.43 mol %	1.54–2.05 mol %
		$\delta^{13}C$	−3.72 to −3.98 ‰PDB	−8.17 to −13.65 ‰PDB
	Mineralogy	Quartz	54 to 68 wt % (13 samples)	56 to 64 wt % (7 samples)
		Feldspar	2 to 12 wt % (13 samples)	2 to 8 wt % (7 samples)
		Clay	24 to 32 wt % (4 samples), 28 to 40 wt % (9 samples)	24 to 32 wt % (7 samples)
		Calcite	0 wt % (13 samples)	2 to 3 wt % (6 samples), 5 wt % (1 sample)
		Ankerite	2 wt % (7 samples), 3 to 5 wt % (6 samples)	0 wt % (6 samples), 3 wt % (1 sample)
	Carbonate cement	$\delta^{13}C$	−2.07 ‰PDB (5 samples)	−4.19 to −2.76 ‰PDB (6 samples)
		$\delta^{18}O$	−10.05 ‰PDB (5 samples)	−9.93 to −6.71 ‰PDB (6 samples)
	XRD clay	Illite + Illite smectite mixed layers	30 to 50 wt % (13 samples)	20 to 50 wt % (7 samples)
		Chlorite	0 to 10 wt % (13 samples)	50 to 60 wt % (7 samples)
		Kaolinite	50 to 80 wt % (13 samples)	0 to 5 wt % (7 samples)
	Physical state	Burial depth	2600–3100 m	2900–3400 m
		Pressure	50–60 MPa	50–60 MPa
		Temperature	110–150 °C	110–150 °C
Caprock	Fracture density		Dense	Sparse
	XRD Clay	Illite + Illite smectite mixed layers	60 to 70 wt % (Well 1–12)	50 to 70 wt % (Well 2–1)
		Chlorite	< 18 wt % (Well 1–12)	Up to 40 wt % (Well 2–1)
		Kaolinite	10 to 20 wt % (Well 1–12)	< 10 wt % (Well 2–1)

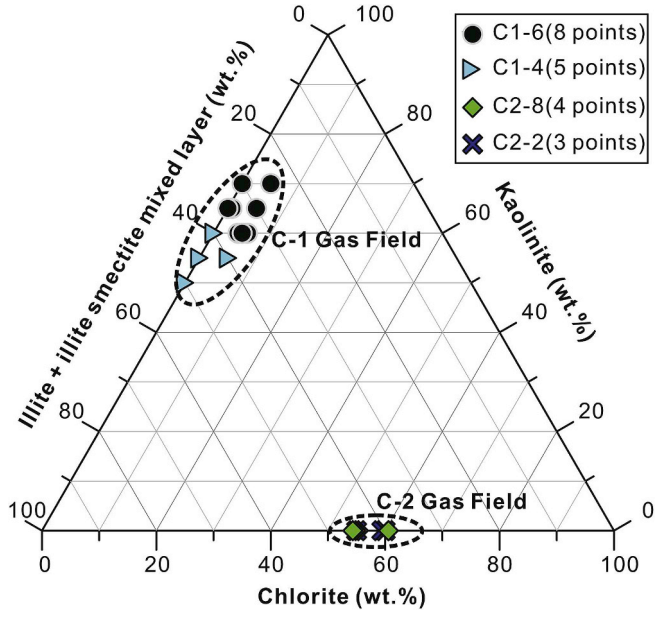

Fig. 7. Results of the XRD analysis on clay minerals of the Upper Miocene sandstone reservoirs in the C-1 and C-2 fields. Note that the C-1 reservoir is rich in kaolinite whereas the C-2 reservoir is rich in chlorite. The proportion of illite and illite/smectite mixed layers is relatively constant at roughly 40 wt%.

4.3. Brine geochemistry

The brine analyses indicates that Na^+/K^+, Ca^{2+}, Mg^{2+}, CO_3^{2-}/HCO_3^-, SO_4^{2-}, and Cl^-, in the four samples of the two fields are the dominant ions (Table 2). The concentration of total dissolved solids (TDS) in the C-2 reservoirs is three times higher than in the C-1 reservoirs, and it is twice as high as seawater. Among major cations, the proportions of both Ca^{2+} and Na^+/K^+ are higher in the C-2 reservoirs, and the Mg^{2+} proportion is higher in the C-1 reservoirs. Of the major anions, the proportion of CO_3^{2-}/HCO_3^- in both fields is higher than that of seawater.

4.4. Pressure data

The pressure data from 6 wells are plotted in Fig. 10. Both fields show overpressure of more than 20 MPa. The fluid pressure in the CO_2-rich C-1 reservoirs is higher, reaching more than 80% of the calculated overburden stress and exceeding the minimum horizontal stress calculated by Liu et al. (2016). Pressure data in C-2 reservoirs are slightly lower and do not exceed 80% of the overburden stress. The pressure data of the reservoirs do not plot on a common fluid gradient.

4.5. Geochemical modelling

The PHREEQC models show that the calcite-chlorite assemblage found in the C-2 reservoirs is stable at low partial pressures of CO_2, corresponding to a maximum of approximately 10 mol% CO_2 in the free-phase gas. Above this CO_2 content, the calcite and chlorite react to dolomite plus kaolinite. Five moles of calcite are consumed for each mole of chlorite.

5. Discussion

The C-1 and C-2 fields are located c.a. 10 km apart, and they are both buried to a depth between 2600 m and 3400 m, with the C-1 reservoirs approximately 300 m shallower. Both fields are of similar stratigraphic age, likely share an overall similar geological history and hence should have had the same mineral assemblage. However, the carbonate minerals and the clay minerals show distinct differences between the two fields and we hypothesize that the difference in mineralogy of the reservoir rock and the caprock between the two fields is related to the pore fluid, in particular to the high concentration of CO_2 physically trapped in the C-1 reservoirs, which leads to the mineral reactions.

5.1. Mineral trapping in the reservoirs

Supercritical CO_2 dissolves in water to form aqueous CO_2 and carbonic acid, then the latter dissociates into H^+ and HCO_3^-/CO_3^{2-}, a process called dissolution trapping which leads to volume reduction of free phase CO_2 and hence increases storage security (Alcalde et al., 2018). Once CO_2 has dissolved in the in-situ brine, the CO_2-rich fluid reacts with the minerals and either dissolves those or precipitates new minerals, the latter process is generally called mineral trapping and leads to the final stage of permanent storage of CO_2. Analogue studies have shown that permanently trapped CO_2 precipitates in stable mineral phases, mainly as carbonate minerals (Gunter et al., 2004; Bickle et al., 2013; De Silva et al., 2015). Alternatively, the increased

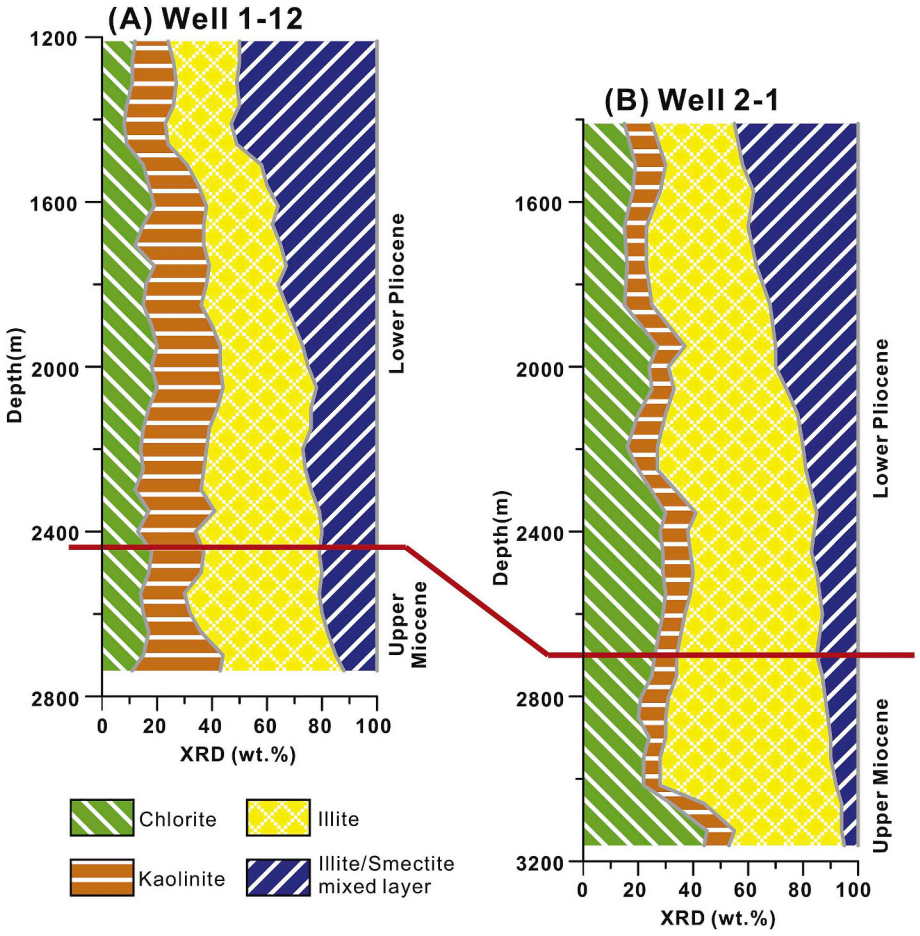

Fig. 8. Clay composition (< 2 μm) of the Pliocene mudstone caprock in wells 1–12 (C-1) and 2–1 (C-2). Note the higher chlorite to Kaolinite ratio in well 2–1. The red line marks the boundary between the Upper Miocene and Lowe Pliocene shale-rich rocks. (For interpretation of the references to colour in this figure legend, the reader is referred to the Web version of this article.)

acidification of the pore water can lead to the dissolution of carbonate minerals, especially during the early stages of CO_2 influx (Wilkinson et al., 2009).

The Upper Miocene reservoirs in the study area have similar amounts of quartz, feldspar, carbonates, and clay. The distinct difference is that there are calcite and chlorite in the C-2 reservoirs but no ankerite and kaolinite, whereas in the C-1 reservoirs there are ankerite and kaolinite but little or no calcite and chlorite. Chlorite is susceptible to acid dissolution and hence the chlorite in the C-1 reservoirs was dissolved when natural CO_2 entered the reservoir and lowered the pH (Armitage et al., 2013; Black and Haese, 2014; Kampman et al., 2014). The tiny amount of chlorite in the C-1 reservoirs can be interpreted as residual chlorite which survived the CO_2-driven dissolution and indicates that chlorite was present in the pre-CO_2 times. Additionally, the calcite also dissolves under acidic conditions. Hence, the CO_2 entering the C-1 reservoirs and lowering the pH is responsible for the dissolution of the chlorite and calcite whereas in C-2 reservoirs, in the reservoir with no or little amounts of CO_2, both mineral phases are still stable. Dissolution of chlorite is suggested to release Mg^{2+} and Fe^{2+} to form the ankerite (Xu et al., 2005; Wilkinson et al., 2009; Heinemann et al., 2013; Kampman et al., 2014), corresponding to a slightly higher Mg^{2+} proportion in the brine of the C-1 reservoirs (Table 2). Kaolinite, which has been reported to be a typical product of chlorite dissolution (Kampman et al., 2014), replaces chlorite as an aluminum-rich phase and ankerite which is more stable under acidic conditions, takes on the cations from the breakdown of the chlorite and replaces calcite as the CO_2 bearing mineral. The reaction can be written as:

$$\underset{\text{Calcite}}{5CO_2} + \underset{}{5CaCO_3} + \underset{\text{Chlorite}}{Mg_5Al_2Si_3O_{10}(OH)_8} = \underset{\text{Dolomite}}{5CaMg(CO_3)_2} + \underset{\text{Kaolinite}}{Al_2Si_2O_5} + \underset{\text{Quartz}}{2H_2O} \quad (1)$$

Note that the reaction as written using the phase compositions from the PHREEQC data base consumes 5 mol of calcite for each mole of chlorite. The C-2 reservoirs do not contain sufficient calcite (approximately 3%) for the measured chlorite (approximately 60% of 30% clay, i.e. 15%) to allow the reaction to run to completion in the C-1 reservoirs, assuming an identical starting composition. The reaction shows that 50% of the CO_2 in the newly formed ankerite is derived from the gas phase, i.e. is net mineral trapping of CO_2.

5.2. Isotope geochemistry

The interpretation, that the newly formed ankerite precipitated due to the presence of the CO_2 in the reservoir, is supported by the isotope geochemistry. Utilizing the oxygen-carbon isotopic fractionation in the system of calcite-water-CO_2 (O'Neil et al., 1969; Deines et al., 1974) the calculated isotopic compositions of the calcite in the C-2 reservoirs were in equilibrium with CO_2 at temperature of 60–100 °C. The range of oxygen and carbon isotopic ratios in the C-2 reservoirs indicates a gradual precipitation of calcite during subsidence at burial depths with reservoir temperatures from at least 60–90 °C, at equivalent reservoir depth between approximately 1100 m and 1800 m, respectively, calculated with recent subsurface temperature data taken from Hao et al. (2000) (Fig. 5).

As no isotope fractionation coefficients for ankerite-water-CO_2 are currently available, geochemically similar dolomite coefficients were utilised. The calculated isotopic compositions of ankerite in the C-1 reservoirs, using the system of dolomite-water-CO_2 (Horita, 2014), are shown in Fig. 9. The measured $\delta^{13}C$ and $\delta^{18}O$ values in the C-1 reservoirs are almost constant at −2 ‰PDB and −10 ‰PDB respectively, implying that the ankerite principally cemented within a narrow

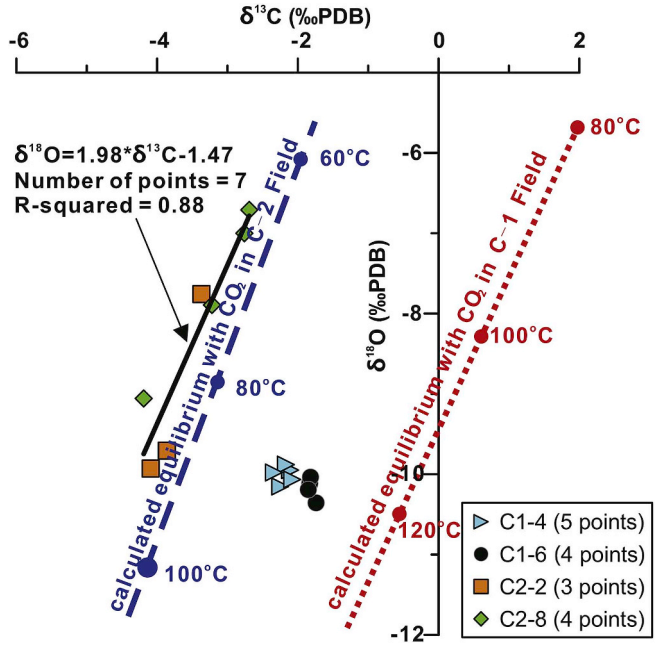

Fig. 9. Stable oxygen and carbon isotopic data for carbonate minerals in the reservoirs of the C-1 and C-2 fields. As shown in Fig. 6, ankerite and calcite are the main carbonate minerals in the C-1 and C-2 reservoirs, respectively. The median values of $\delta^{13}CO_2$ are −3.86‰ PDB and −9.05‰ PDB in the C-1 and C-2 fields, respectively. Using the oxygen and carbon isotopic fractionation in the systems of calcite-water-CO_2 (O'Neil et al., 1969; Deines et al., 1974) and dolomite-water-CO_2 (Horita, 2014), the carbonate mineral equilibrium with CO_2 in the C-2 and C-1 reservoirs were calculated respectively.

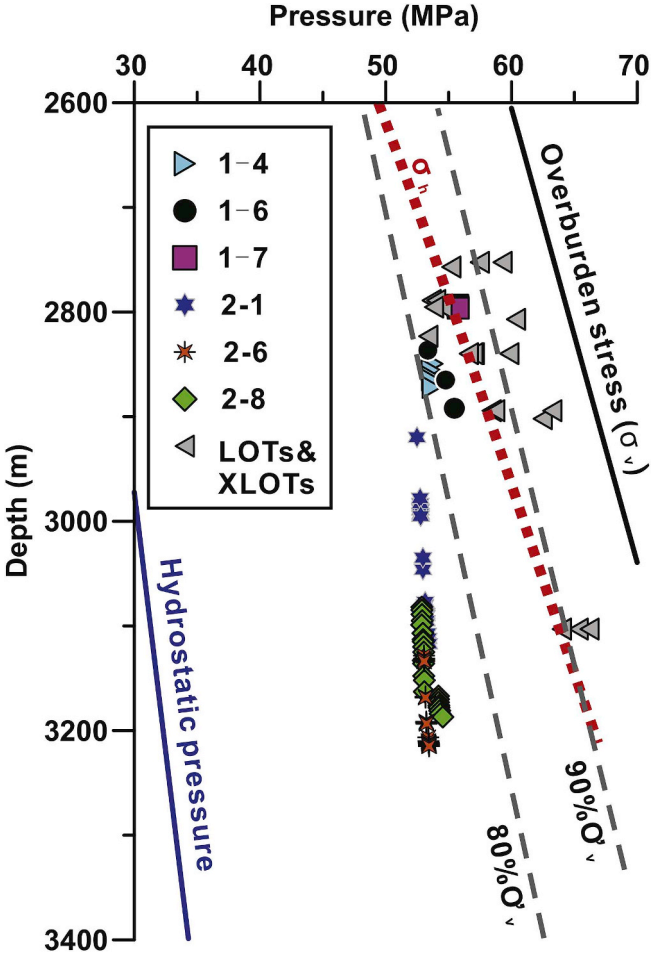

Fig. 10. Fluid pressure versus depth in the C-1 and C-2 fields. σ_v is the overburden stress, and σ_h is the least horizontal stress derived from the leak-off tests and extended leak-off tests (LOTs & XLOT) of Liu et al. (2016). Note that the pressure of the C-1 field exceeds 80%σ_v and reaches the threshold value of hydraulic fracturing. The overburden stress and the hydrostatic pressure were calculated using bulk rock density wireline data and formation water density, respectively.

temperature range, here interpreted as the depth at which the CO_2 charged the reservoirs. The $\delta^{13}C$ and $\delta^{18}O$ values of ankerite in the C-1 reservoirs do not fall on the calculated line (Fig. 9), implying that either the source of $\delta^{13}C$ or $\delta^{18}O$ in the C-1 reservoirs has changed with time or that the dolomite isotope fractionation coefficient for ankerite is not accurate. The measured $\delta^{18}O$ values are close to the calculated values at the temperature of approximately 120 °C, which is close to the present-day reservoir temperature of the C-1 field.

5.3. Pressure system

Physical trapping of CO_2 occurs when free CO_2 is immobilized in the reservoir pore of structural/stratigraphic traps (Gunter et al., 2004; Bachu et al., 2007; Heinemann et al., 2016). One risk for physical CO_2 trapping is hydraulic fracturing, which can lead to reservoirs losing significant volumes of the stored CO_2 (Song and Zhang, 2013; Miocic et al., 2016; Edlmann et al., 2016). Hydraulic fracturing occurs if the fluid pressure exceeds the minimum horizontal stress and triggers the opening of pathways, which allow the fluid to migrate out of the reservoir. As a consequence, the fluid pressure then drops until the pathways close.

Little is known about the source of overpressure in the fields. Disequilibrium compaction, the most common source of overpressure in rapidly buried low-permeability clastic sediments, certainly had its impact but cannot, according to Luo et al. (2003), explain the high reservoir pressures. Luo et al. (2003) suggest pressure transfer from deeper reservoirs via faults, a process often referred to as lateral transfer (Yardley and Swarbrick, 2000), as an explanation for the high reservoir pressures. Additionally, the reaction of smectite to illite, which is common in young basins with high temperature gradients, can lead to a collapse of the rock matrix which additionally generates overpressure (Lahann and Swarbrick, 2011). However, a more detailed

Table 2
Composition of brines in the C-1 and C-2 reservoirs and seawater. Brine samples were obtained from drill stem tests (DST) and modular dynamic tests (MDT).

Fields	Wells	Depth (m)	Sample sources	CO_3^{2-}/HCO_3^-	Cl^-	SO_4^{2-}	Ca^{2+}	Mg^{2+}	$K^+ + Na^+$	TDS	pH
				(mg/L)							
C-2 field	C2-1	3090	MDT	5445	28409	4502	60	5	22550	60971	8.07
C-1 field	C1-6	2819–2836.5	DST	9805	5625	114	29	8	7348	22929	7.08
	C1-14A	2910–2918	DST	181	2285	349	28	13	1661	4517	6.47
	C1−14B	2933–2963	DST	3083	5825	72	32	9	4923	13944	7.09
Seawater		/	/	108	19352	2712	412	1284	11183	35000	8.1

analysis of the petrophysical data is required to better understand the origin of the extreme overpressure in the Yinggehai Basin.

Both fields show significant overpressure with pressure data in the C-1 reservoirs indicating more overpressure compared to the C-2 reservoirs, although the C-1 reservoirs are shallower. This indicates that the C-1 and C-2 reservoirs are not in communication. The pressure in the C-1 reservoirs exceeds 80% of overburden stress (σ_v), whereas the C-2 reservoirs pressure remains slightly lower. At least in the current state, hydraulic fracturing in the C-1 reservoirs is more likely than in the C-2 reservoirs. The reason for the difference in overpressure between C-1 and C-2 reservoirs is uncertain. Three explanations are possible: (a) C-1 reservoirs have been connected to a more overpressured gas source in the subsurface and hence has been charged with higher pressures (Luo et al., 2003); (b) C-2 reservoirs have suffered a seal breach event and is currently re-charging; or (c) C-1 reservoirs have maintained its pressure during uplift and is still holds the fluid pressure from its original (deeper) burial depth (Liu et al., 2015).

The presence of such overpressure levels makes CO_2 storage operations very challenging. The overpressured reservoirs have to be drilled and enough fluid, either hydrocarbons or brine, have to be produced to allow CO_2 injection. If disequilibrium compaction is the main reason for the overpressure, the now CO_2-filled reservoir will equilibrate with the high pressure shales surrounding the reservoirs hence making hydraulic fracturing in the future likely.

5.4. Caprock stability and reaction

The overall proportion of illite and illite/smectite mixed layers in the caprocks of the two fields are relatively similar, which supports the idea that the mineralogy of both fields was similar before the CO_2 entered the C-1 reservoirs. If the shale in the C-2 field is regarded as the 'default' shale, a comparison with the C-1 reservoirs shows a relative depletion in chlorite and an enrichment with kaolinite. The breakdown of chlorite in the presence of CO_2 has been discussed in the C-1 reservoir sandstones already and it is possible that the same reaction also took place in the caprock. We suggest that overpressure exceeding the fracture pressure of the C-1 caprock triggered the opening of fractures and CO_2 rich fluid migrated from the reservoir into the overlying shales. Here, the fluid reacted with and dissolved the chlorite and precipitated kaolinite.

Whether hydraulic fracturing or capillary leakage is the process responsible for the caprock failure is unknown; the fact is, however, that no permanent leakage pathway has been opened and that there is still a significant volume of CO_2 in the C-1 reservoir.

6. Summary

The investigation of petrological, stable isotope, and pressure data has given important insights into geological history of CO_2-rich reservoirs in the Yinggehai Basin. The isotope data show gradual precipitation of calcite during burial in the C-2 reservoirs and we hypothesize that the same calcite was also deposited in the nearby C-1 reservoirs. Calcite precipitation stopped at a depth of around 1800 m and no further carbonate precipitation occurred during the ongoing subsidence. At some point during the diagenesis, the CO_2 dissolved in the reservoir fluid, lowering the pH and shifting the geochemical equilibrium in the C-1 reservoirs. As a consequence, calcite and chlorite dissolved and ankerite and kaolinite were precipitated. It is likely that some of the CO_2 migrated into the shale-dominated C-1 caprock where chlorite was dissolved and kaolinite precipitated.

7. Conclusion

- The Upper Miocene siliciclastic reservoirs and overlying caprocks in the Yinggehai Basin retain CO_2 as natural reservoirs. Although the reservoirs are highly overpressured and engineered CO_2 storage operations might be challenging; nevertheless, they represent excellent analogues to study the long-term effect of CO_2 storage on both reservoir and caprocks.
- CO_2 charging of the C-1 reservoirs triggered a reaction between pre-existing calcite and chlorite, precipitating ankerite and kaolinite. This has been modeled in PHREEQC, albeit in a Fe-free system, confirming the viability of the reaction. Modelling indicates that 5 mol of CO_2 are sequestered for every mole of chlorite reacted; half of the ankerite CO_2 is sequestered CO_2, the other half is derived from the reacted calcite.
- There is evidence for CO_2 induced mineral reactions in the caprock indicating CO_2 migration from the reservoir into the overlying shale. Whether this is due to hydraulic fracturing or capillary leakage is not known; however, significant overpressure in the reservoirs suggest that the shale caprocks have preserved their integrity to retain significant volumes of CO_2 and hence it is concluded that the mineral reactions have not further compromised the integrity of the caprock.

Acknowledgements

This research was supported by the 111 project (No. B14031), the National Natural Science Foundation of China (No. 41672141 and No. 41702157) and the Young scholars development fund of SWPU (No. 201699010085). NH has received funding from the European Union's H2020 Accelerating CCS technologies and UKCCSRC (EP/P026214/1). SH is funded by EPSRC and NERC. We appreciate the collaboration and enthusiastic support of Hongjun Yang, Jianxiang Pei, Antao Xiao, Lifeng Wang, Huolan Zhang, and Nengping Ai at the Zhanjiang Branch of CNOOC Ltd.

Appendix A. Supplementary data

Supplementary data to this article can be found online at https://doi.org/10.1016/j.marpetgeo.2019.03.018.

References

Alcalde, J., Flude, S., Wilkinson, M., Johnson, G., Edlmann, K., Bond, C.E., Scott, V., Gilfillan, S.M., Ogaya, X., Haszeldine, R.S., 2018. Estimating geological CO2 storage security to deliver on climate mitigation. Nat. Commun. 9. https://doi.org/10.1038/s41467-018-04423-1.

Armitage, P.J., Faulkner, D.R., Worden, R.H., 2013. Caprock corrosion. Nat. Geosci. 6, 79–80. https://doi.org/10.1038/ngeo1716.

Bachu, S., Bonijoly, D., Bradshaw, J., Burruss, R., Holloway, S., Christensen, N.P., Mathiassen, O.M., 2007. CO2 storage capacity estimation: methodology and gaps. International Journal of Greenhouse Gas Control 1, 430–443. https://doi.org/10.1016/s1750-5836(07)00086-2.

Boden, T.A., Andres, R.J., Global, Gregg Marland, 2017. Regional, and National Fossil-Fuel CO2 Emissions (1751-2014) (V. 2017). Carbon Dioxide Information Analysis Center (CDIAC), Oak Ridge National Laboratory (ORNL), Oak Ridge, TN (United States).

Bickle, M.J., 2009. Geological carbon storage. Nat. Geosci. 2, 815–818. https://doi.org/10.1038/ngeo687.

Bickle, M., Kampman, N., Wigley, M., 2013. Natural Analogues: Rev. Mineral. Geochem. 77, 15–71. https://doi.org/10.2138/rmg.2013.77.2.

Black, J.R., Haese, R.R., 2014. Chlorite dissolution rates under CO2 saturated conditions from 50 to 120 °C and 120 to 200 bar CO2. Geochem. Cosmochim. Acta 125, 225–240. https://doi.org/10.1016/j.gca.2013.10.021.

Cao, L.C., Jiang, T., Wang, Z.F., Zhang, Y.Z., Sun, H., 2015. Provenance of upper Miocene sediments in the Yinggehai and qiongdongnan basins, northwestern South China sea: evidence from REE, heavy minerals and zircon U-Pb ages. Mar. Geol. 361, 136–146. https://doi.org/10.1016/j.margeo.2015.01.007.

De Silva, G.P.D., Ranjith, P.G., Perera, M.S.A., 2015. Geochemical aspects of CO2 sequestration in deep saline aquifers: a review. Fuel 155, 128–143. https://doi.org/10.1016/j.fuel.2015.03.045.

Deines, P., Langmuir, D., Harmon, R.S., 1974. Stable carbon isotope ratios and existence of a gas-phase in evolution of carbonate ground waters. Geochem. Cosmochim. Acta 38, 1147–1164. https://doi.org/10.1016/0016-7037(74)90010-6.

Edlmann, K., Bensabat, J., Niemi, A., Haszeldine, R.S., McDermott, C.I., 2016. Lessons learned from using expert elicitation to identify, assess and rank the potential leakage scenarios at the Heletz pilot CO2 injection site. International Journal of Greenhouse Gas Control 49, 473–487.

Gong, Z.S., Li, S.T., 1997. Continental Margin Basin Analysis and Hydrocarbon

Accumulation of the Northern South China Sea: Beijing. Science Press, pp. 193–256.
Gunter, W.D., Bachu, S., Benson, S., 2004. The Role of Hydrogeological and Geochemical Trapping in Sedimentary Basins for Secure Geological Storage of Carbon Dioxide. vol. 233. Geological Society, London, Special Publications, pp. 129–145.
Hao, F., Li, S.T., Gong, Z.S., Yang, J.M., 2000. Thermal regime, interreservoir compositional heterogeneities, and reservoir-filling history of the Dongfang gas field, Yinggehai basin, South China Sea: evidence for episodic fluid injections in overpressured Basins. AAPG (Am. Assoc. Pet. Geol.) Bull. 84, 607–626.
Heinemann, N., Wilkinson, M., Haszeldine, R.S., Fallick, A.E., Pickup, G.E., 2013. CO2 sequestration in a UK North Sea analogue for geological carbon storage. Geology 41, 411–414. https://doi.org/10.1130/g33835.1.
Heinemann, N., Stewart, R.J., Wilkinson, M., Pickup, G., Haszeldine, R.S., 2016. Hydrodynamics in subsurface CO2 storage: tilted contacts and increased storage security. International Journal of Greenhouse Gas Control 54, 322–329.
Heinemann, N., Haszeldine, R.S., Shu, Y., Wilkinson, M., 2017. CO2 storage as dispersed trapping in proximal areas of the Pearl River Mouth Basin offshore Guangdong. China. Energy Proc 114, 4436–4443.
Heinemann, N., Haszeldine, R.S., Shu, Y., Stewart, R.J., Scott, V., Wilkinson, M., 2018. CO2 sequestration with limited sealing capability: a new injection and storage strategy in the Pearl River Mouth Basin (China). Int. J. Greenhouse Gas Control 68, 230–235.
Hillier, S., 2003. Quantitative Analysis of Clay and Other Minerals in Sandstones by X-Ray Powder Diffraction (XRPD): Clay Mineral Cements in Sandstones (Special Publication Number 34 of the International Association of Sedimentologist). Blackwell Science, Oxford.
Horita, J., 2014. Oxygen and carbon isotope fractionation in the system dolomite-water-CO2 to elevated temperatures. Geochem. Cosmochim. Acta 129, 111–124. https://doi.org/10.1016/j.gca.2013.12.027.
Huang, B., Tian, H., Huang, H., Yang, J., Xiao, X., Li, L., 2015. Origin and accumulation of CO2 and its natural displacement of oils in the continental margin basins, northern South China Sea. AAPG (Am. Assoc. Pet. Geol.) Bull. 99, 1349–1369. https://doi.org/10.1306/02091514125.
Huang, B.J., Xiao, X.M., Dong, W.L., 2002. Multiphase natural gas migration and accumulation and its relationship to diapir structures in the DF1-1 gas field. South China Sea: Mar. Petrol. Geol. 19, 861–872. https://doi.org/10.1016/S0264-8172(02)00109-5.
Huang, B.J., Xiao, X.M., Zhu, W.L., 2004. Geochemistry, origin, and accumulation of CO2 in natural gases of the Yinggehai Basin, offshore South China Sea. AAPG (Am. Assoc. Pet. Geol.) Bull. 88, 1277–1293. https://doi.org/10.1306/04120403045.
IPCC, 2005. IPCC Special Report on Carbon Dioxide Capture and Storage. Cambridge University Press, Cambridge.
Jiang, T., Cao, L., Xie, X., Wang, Z., Li, X., Zhang, Y., Zhang, D., Sun, H., 2015a. Insights from heavy minerals and zircon U-Pb ages into the middle Miocene-Pliocene provenance evolution of the Yinggehai Basin, northwestern South China Sea. Sediment. Geol. 327, 32–42. https://doi.org/10.1016/j.sedgeo.2015.07.011.
Jiang, T., Xie, X., Chen, H., Wang, Z., Li, X., 2015b. Geochemistry of pore water and associated diagenetic reactions in the diapiric area of Yinggehai Basin, northwestern South China sea. J. Earth Sci. 26, 306–316.
Kampman, N., Bickle, M., Wigley, M., Dubacq, B., 2014. Fluid flow and CO2-fluid-mineral interactions during CO2-storage in sedimentary basins. Chem. Geol. 369, 22–50. https://doi.org/10.1016/j.chemgeo.2013.11.012.
Lahann, R.W., Swarbrick, R.E., 2011. Overpressure generation by load transfer following shale framework weakening due to smectite diagenesis. Geofluids 11, 362–375. https://doi.org/10.1111/j.1468-8123.2011.00350.x.
Lei, C., Ren, J., Clift, P.D., Wang, Z., Li, X., Tong, C., 2011. The structure and formation of diapirs in the Yinggehai-Song Hong basin, South China sea. Mar. Petrol. Geol. 28, 980–991. https://doi.org/10.1016/j.marpetgeo.2011.01.001.
Liu, R., 2016. Overpressure Expulsion and its Influences on Hydrocarbon Accumulation in the Dongfang Area of Yinggehai Basin, Northwestern South China Sea, Doctor's Thesis. China University of Geosciences, Wuhan, pp. 79–82.
Liu, R., Liu, J., Zhu, W., Hao, F., Xie, Y., Pei, J., Wang, L., 2015. Expulsion process of overpressure fluids indicated by vertical venting structures in the Dongfang area of the Yinggehai Basin. offshore South China Sea: Mar. Petrol. Geol. 66, 848–860. https://doi.org/10.1016/j.marpetgeo.2015.07.024.
Liu, R., Liu, J., Zhu, W., Hao, F., Xie, Y., Wang, Z., Wang, L., 2016. In situ stress analysis in the Yinggehai Basin, northwestern South China Sea: implication for the pore pressure-stress coupling process. Mar. Petrol. Geol. 77, 341–352. https://doi.org/10.1016/j.marpetgeo.2016.06.008.
Luo, X., Dong, W., Yang, L., Yang, W., 2003. Overpressure mechanisms in the Yinggehai Basin, South China sea. AAPG Bull. 87, 629–645. https://doi.org/10.1306/10170201045.
Moore, D.M., Reynolds, R.C., 1997. X-ray Diffraction and the Identification and Analysis of Clay Minerals. Oxford University Press, Oxford.
Miocic, J.M., Gilfillan, S.M.V., Roberts, J.J., Edlmann, K., McDermott, C.I., Haszeldine, R.S., 2016. Controls on CO2 storage security in natural reservoirs and implications for CO2 storage site selection. International Journal of Greenhouse Gas Control 51, 118–125. https://doi.org/10.1016/j.ijggc.2016.05.019.
Morley, C.K., 2002. A tectonic model for the Tertiary evolution of strike-slip faults and rift basins in SE Asia. Tectonophysics 347, 189–215. https://doi.org/10.1016/s0040-1951(02)00061-6.
Morley, C.K., 2013. Discussion of tectonic models for Cenozoic strike-slip fault-affected continental margins of mainland SE Asia. J. Asian Earth Sci. 76, 137–151. https://doi.org/10.1016/j.jseaes.2012.10.019.
O'Neil, J.R., Clayton, R.N., Mayeda, T.K., 1969. Oxygen isotope fractionation in divalent metal carbonates. J. Chem. Phys. 51, 5547–5558. https://doi.org/10.1063/1.1671982.
Song, J., Zhang, D.X., 2013. Comprehensive review of caprock-sealing mechanisms for geologic carbon sequestration. Environ. Sci. Technol. 47, 9–22. https://doi.org/10.1021/es301610p.
Sun, M., Wang, H., Liao, J.H., Gan, H.J., Xiao, J., Ren, J.F., Zhao, S.E., 2014. Sedimentary characteristics and model of gravity flow depositional system for the first member of Upper Miocene Huangliu Formation in Dongfang area, Yinggehai basin, northwestern South China Sea. J. Earth Sci. 25, 506–518. https://doi.org/10.1007/s12583-014-0451-5.
The Netherlands Environmental Assessment Agency, 2007. Global CO2 Emissions: Increase Continued in 2007. http://www.pbl.nl/en/publications/2008/GlobalCO2emissionsthrough2007.
Tong, C., Xie, Y., Huang, Z., Ma, Y., 2015. Geochemical behaviors of HPHT gas reservoirs in the Yinggehai Basin and the efficient gas accumulation mode at the basin's diapir flanks. Nat. Gas. Ind. 35, 1–11 (in Chinese with English abstract).
Wilkinson, M., Haszeldine, R.S., Fallick, A.E., Odling, N., Stoker, S.J., Gatliff, R.W., 2009. CO2–mineral reaction in a natural analogue for CO2 storage — implications for modelling. J. Sediment. Res. 79, 486–494. https://doi.org/10.2110/jsr.2009.052.
Xie, Y.H., Huang, B.J., 2014. Characteristics and accumulation mechanisms of the Dongfang 13-1 high temperature and overpressured gas field in the Yinggehai Basin, the South China Sea: Science China. Earth Sci. 44, 1731–1739. https://doi.org/10.1007/s11430-014-49340.
Xu, T., Apps, J.A., Pruess, K., 2005. Mineral sequestration of carbon dioxide in a sandstone–shale system. Chem. Geol. 217, 295–318. https://doi.org/10.1016/j.chemgeo.2004.12.015.
Yardley, G.S., Swarbrick, R.E., 2000. Lateral transfer: a source of additional overpressure? Mar. Petrol. Geol. 17, 523–537. https://doi.org/10.1016/S0264-8172(00)00007-6.
Zhang, H., Pei, J., Zhang, Y., Jiang, C., Zhu, J., Ai, N., Hu, Q., Yu, J., 2013. Overpressure Reservoirs of the Huangliu Formation of the Dongfang Area, Yinggehai Basin. vol. 40. Petroleum Exploration and Development, South China Sea, pp. 305–316. https://doi.org/10.1016/S1876-3804(13)60037-3.
Zhou, D., Zhao, Z., Liao, J., Sun, Z., 2011. A primarily assessment on CO2 storage capacity in the Pearl River Mouth Basin offshore Guangdong China. Int. J. Greenhouse Gas Control 5, 308–317.
Zhu, M., Graham, S., McHargue, T., 2009. The Red River fault zone in the Yinggehai Basin, South China sea. Tectonophysics 476, 397–417. https://doi.org/10.1016/j.tecto.2009.06.015.